

# RSC Advances



This is an *Accepted Manuscript*, which has been through the Royal Society of Chemistry peer review process and has been accepted for publication.

*Accepted Manuscripts* are published online shortly after acceptance, before technical editing, formatting and proof reading. Using this free service, authors can make their results available to the community, in citable form, before we publish the edited article. This *Accepted Manuscript* will be replaced by the edited, formatted and paginated article as soon as this is available.

You can find more information about *Accepted Manuscripts* in the [Information for Authors](#).

Please note that technical editing may introduce minor changes to the text and/or graphics, which may alter content. The journal's standard [Terms & Conditions](#) and the [Ethical guidelines](#) still apply. In no event shall the Royal Society of Chemistry be held responsible for any errors or omissions in this *Accepted Manuscript* or any consequences arising from the use of any information it contains.

## ARTICLE

## Corrosion resistance of graphene directly and locally grown on bulk nickel substrate by laser radiation

Cite this: DOI: 10.1039/x0xx00000x

X.H. Ye,<sup>a</sup> F. Yu,<sup>b</sup> M. Curioni,<sup>b</sup> Z. Lin,<sup>a</sup> H.J. Zhang,<sup>a</sup> H.W. Zhu,<sup>a</sup> Z. Liu,<sup>b</sup> and M.L. Zhong\*<sup>a</sup>

Received 00th January 2012,

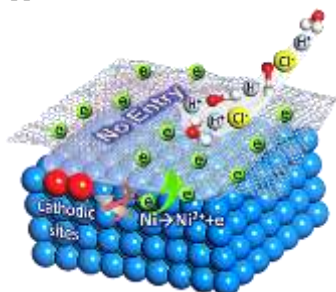
Accepted 00th January 2012

DOI: 10.1039/x0xx00000x

[www.rsc.org/](http://www.rsc.org/)

### Table of Contents

Graphene grown by laser is superior at resisting the acid corrosive environment for realizing the real application in anti-corrosion field.



## ARTICLE

## Corrosion resistance of graphene directly and locally grown on bulk nickel substrate by laser radiation

Cite this: DOI: 10.1039/x0xx00000x

X.H. Ye,<sup>a</sup> F. Yu,<sup>b</sup> M. Curioni,<sup>b</sup> Z. Lin,<sup>a</sup> H.J. Zhang,<sup>a</sup> H.W. Zhu,<sup>a</sup> Z. Liu,<sup>b</sup> and M.L. Zhong\*<sup>a</sup>Received 00th January 2012,  
Accepted 00th January 2012

DOI: 10.1039/x0xx00000x

www.rsc.org/

We report the anticorrosion capability of graphene directly and locally grown on bulk nickel substrate by a high power laser beam at room temperature. The anticorrosive performance of the locally laser-grown graphene on Ni, together with Ni covered graphene transferred from CVD method and bare Ni, was investigated by electrochemical measurements and immersion tests. The corrosion rate evaluated from potentiodynamic polarizations was 4.5 times lower than that for bare Ni, and the corrosion potential was increased by 126 mV. Electrochemical impedance spectroscopy (EIS) measurements complemented the potentiodynamic results and indicated significant improvement in corrosion resistance in the presence of *in-situ* grown graphene. The *in-situ* grown graphene could protect the underlying substrate effectively, mainly due to its strong interaction with substrate, and excellent barrier properties. This laser fabrication of graphene directly and locally on bulk substrate provides a promising and workable method to protect the metals from corrosion.

### Introduction

Corrosion is a chemical or electrochemical reaction at the metal/electrolyte interface. Each year, the corrosion of metals causes substantial financial loss and sometimes even disasters. It is of strategic significance and economic impact to develop methods to inhibit or control the corrosion of metals. The use of available protective coatings is an effective, convenient and economic method. These coatings are usually made of inert materials, with the function of separating the metals from the corrosive environment. So far, many organic and polymeric coatings have been employed to protect metals against corrosion.<sup>1-3</sup> These organic and polymeric coatings normally change the metal properties, such as conductivity and optical properties. It is very helpful to develop a transparent and conductive coating as an alternate.

Graphene is a single layer or few layers of carbon atoms, tightly packed into a two-dimensional (2D) honeycomb lattice. It has attracted a tremendous amount of attention and research focus since it was successfully exfoliated from highly oriented pyrolytic graphite (HOPG) in 2004.<sup>4-7</sup> Novoselov has ever proposed<sup>4</sup> "Graphene is highly inert, and so can also act as a corrosion barrier against water and oxygen diffusion. Given that it can be grown directly on the surface of almost any metal under the right conditions, it could form a protective conformal layer, that is, it could be used on complex surfaces". The unique

properties of graphene, *e.g.* extremely high carrier mobility, chemical stability and excellent impermeability,<sup>8-11</sup> make it possible to be the ideal corrosion inhibiting coating on applications such as aircraft and ship components.<sup>12-19</sup> Several pioneering studies have demonstrated that graphene coatings are excellent anticorrosion barriers for metals. Bunch *et al.*<sup>11</sup> firstly reported that a monolayer graphene membrane was impermeable to standard gases, including helium. This work opened up a new route to realize the practical application of graphene. Then some efforts were reported on using graphene to inhibit corrosion and oxidation of metals. Chen *et al.*<sup>12</sup> demonstrated that CVD-grown graphene can effectively protect Cu and Cu/Ni foils from thermal oxidation in air at 200 °C for 4 h and wet oxidation by 30% H<sub>2</sub>O<sub>2</sub>. In a closely related study, Nayak *et al.*<sup>13</sup> reported a similar anticorrosion effect of graphene films grown by CVD to protect the Ni foil from air oxidation. Some other studies employed the electrochemical corrosion to study the anticorrosion performance of graphene. Chang *et al.*<sup>14</sup> reported that polyaniline/graphene composites displayed outstanding barrier properties against O<sub>2</sub> and H<sub>2</sub>O as evidenced by the highest and lowest values of corrosion potential and corrosion current density (which corresponds to a lower corrosion rate), respectively. Prasai and co-workers<sup>15</sup> reported a detailed study on the anticorrosion property of CVD-grown as well as transferred graphene for electrochemical

corrosion of Cu and Ni foils. Their results showed that copper foil coated with graphene grown by CVD were corroded 7 times slower compared to the corrosion rate of bare copper foil. Nickel foil surfaces with an *in-situ* grown multilayer graphene film were corroded much slower than nickel surfaces with four layers of mechanically transferred graphene. Previous studies showed that graphene is an effective anticorrosion barrier against short-term oxidation of metals. Zhou *et al.*<sup>16</sup> investigated the long-term oxidation at room temperature of copper covered by a graphene coating. After 6 months of exposure in air, the graphene-coated copper foil had a higher degree of oxidation than uncoated foil. They considered that the corrosion enhancement effect of graphene was attributed to its ability to promote electrochemical corrosion of copper in the long-term.

These previous works mainly investigated the CVD-grown graphene and the protection of Cu or Ni foils usually with a few dozen micrometres in thickness from the harsh environment. As well known, CVD-growth of graphene, as a widely used graphene synthesis approach, occurs normally in a tube furnace at a temperature around 1000 °C (taking several hours for heating and then cooling) and usually on Cu or Ni foil substrates. These two preconditions will significantly limit the application potential of graphene for anti-corrosion applications. Recently, we have ever reported a new approach for direct fabrication of graphene on bulk Ni substrate by laser direct irradiation at room temperature.<sup>20</sup> A high power diode laser beam was employed to grow graphene with a high growth rate, 28.8 cm<sup>2</sup>/min. By rectangular laser beam or multi-pass, a large area synthesis of graphene on Ni substrate is possible. An important fact is that graphene can be grown directly and locally on bulk Ni substrate surface with any dimension at any location wherever necessary. This indicates a good potential for graphene as an effective local anti-corrosion treatment.

In this paper, we focused on the anti-corrosion capacity of graphene grown on bulk Ni substrate by this laser approach. HCl (aq) was chosen as the corrosive solution instead of 3.5% NaCl, H<sub>2</sub>O or O<sub>2</sub> as previously reported. Nickel is a corrosion-resistant material in neutral and alkaline system, due to the passive film formed on the nickel surface. Once nickel immersed in acidic environment, the passive film is dissolved. Hence, HCl (aq) would be the appropriate solution for investigating the corrosion resistance of graphene-covered nickel. In addition to the sample with laser grown graphene covered on Ni surface, two more samples were used for comparison under the same corrosion conditions: Ni sample with transferred graphene grown by conventional CVD approach, and bare Ni sample. The corrosion behaviours of all these three samples were investigated by electrochemical measurements and immersion tests. The topography and microstructure of all above samples before and after the corrosion process were characterized in order to study the mechanism of graphene corrosion.

## Experimental

### Graphene formation on nickel by laser process

Graphene was obtained by laser irradiation directly.<sup>20</sup> A 4000W diode laser was employed to scan the pre-coated carbon source on the nickel sheet (five-millimetre-thick). By this approach, the substrate surface together with the as-coated carbon is heated at a high rate, forming a large-area bath and then cools down. When the laser was shut off, graphene could be available immediately, within less than 1min. The formation of graphene was implemented by the diode laser with a flat-top beam of 16×1 mm<sup>2</sup>. The laser power density was 1.87×10<sup>3</sup> W/cm<sup>2</sup>, and the scanning rate was 18 cm/min with 25 L/min argon (99.99%) as shielding gas. The nickel sheet with graphene was cut into small pieces of 5×5×5 mm<sup>3</sup>.

### Graphene transferred onto nickel surface

Graphene films grown on copper via atmospheric CVD were used as a comparison. Graphene films were provided by ACS material LLC. The copper foils were etched away with FeCl<sub>3</sub>/HCl aqueous solution. The graphene films (25×25 mm<sup>2</sup>) were then transferred onto the nickel substrate (50×50×5 mm<sup>3</sup>). The nickel sheet with graphene was cut into small pieces of 5×5×5 mm<sup>3</sup>.

### Electrochemical corrosion measurement and immersion test

HCl (aq) solutions of 0.05, 0.1 and 0.5 M were used as the corrosive environments. The corrosion resistance was investigated by an electro-chemical measurement system (CHI601D). A saturated calomel electrode (SCE) was used as a reference electrode, and a platinum electrode was used as auxiliary electrode. The potentiodynamic polarization curves were obtained by sweeping the potential from -900 mV to +500 mV using a scan rate of 1.0 mV/s. For electrochemical impedance spectroscopy (EIS), an AC perturbation of ±10 mV over the open circuit potential was applied over a frequency range from 10<sup>5</sup> to 10<sup>-2</sup> Hz, recording 12 points per decade. EIS spectra were acquired after 1 h of immersion in 0.5 M HCl (aq).

### Characterisation of graphene

The topography and structure of the samples before and after electrochemical corrosion tests were characterized by scanning electron microscopy (SEM, LEO-1530) with an energy dispersive X-ray spectroscopy (EDS), transmission electron microscopy (TEM, JEOL-2011), 532 nm Raman imaging spectroscopy (Nanophoton, Raman-11), and 514 nm Raman spectroscopy (Renishaw 2000).

## Theory

Based on the linear fitting of polarization curves, one can obtain the important reaction kinetic parameters, *i.e.* corrosion current density ( $i_{corr}$ ), corrosion potential ( $E_{corr}$ ), corrosion rate (CR) and polarization resistance ( $R_p$ ).<sup>14,15,21-23</sup>

$$E_{corr} = a_a + b_a \log i_{corr} \quad (1)$$

$$E_{corr} = a_c + b_c \log i_{corr} \quad (2)$$

$$CR = \frac{K \times i_{corr} \times M}{\rho \times V} \quad (3)$$

$$R_p = \frac{b_a \times b_c}{2.303 \times (b_a + b_c) \times i_{corr}} \quad (4)$$

where  $a_a$ ,  $b_a$ ,  $a_c$  and  $b_c$  are the anodic and cathodic intercept and slopes ( $\Delta E/\Delta \log i$ ) respectively,  $K$  is a constant (3270),  $M$  is the molecular weight (58.7 g/mol),  $V$  is the valence (2), and  $\rho$  is the density (8.9 g/cm<sup>3</sup>). A higher free corrosion potential means a higher capability to resist corrosive environments.  $R_p$  reflects the kinetics of the corrosion reactions. Generally, a lower  $i_{corr}$ , CR and a higher  $E_{corr}$ ,  $R_p$  indicate better protection in corrosive environment.

EIS is a versatile tool to elucidate the degradation mechanism of corrosion in both of qualitative and quantitative insight. Unlike potentiodynamic polarization, EIS is non-destructive for the corroding surface since only a small-amplitude sinusoidal potential is applied, and therefore faradic currents are substantially smaller compared to those associated to potentiodynamic polarization. In order to obtain the impedance spectra, the ratio between the amplitude of the applied potential signal and the measured current response at each frequency gives the impedance modulus spectrum, whereas the difference in phase between the two signals provides the phase shift spectrum (Bode plots). Qualitative information can be extracted by examining the shape of Bode or Nyquist plots, and quantitative data can be obtained by equivalent circuit fitting.<sup>24,25</sup>

## Results and discussion

### Graphene growth and transfer

Graphene was obtained by laser irradiation directly.<sup>20</sup> In this approach, the substrate surface together with the as-coated carbon is heated and cooled down rapidly. Once the laser was shut off, the graphene was obtained on the Ni surface immediately, as shown in Fig. 1a and b. In contrast, the CVD-grown graphene films were artificially transferred onto the nickel substrate, as shown in Fig. 1c. The *in-situ* grown graphene (labelled “Gr”) and transferred graphene (labelled “Tr”) have been characterized by SEM, TEM and Raman. Fig. 1d and g show the topographies of graphene *in-situ* grown on nickel by laser radiation and transferred onto nickel surface. It can be seen that the wrinkles of Gr is more than that of Tr, owing to the different thermal expansion coefficients between the nickel and graphene.<sup>26</sup> In Fig. 1g, the polishing scratches of Ni were observed, while the scratches did not exist in Fig. 1d. The difference owed to that the surface remained the same during the transfer process, including the scratches, but the remelting of Ni was caused during laser process. Fig. 1c and h give the layer number directly by the high resolution TEM images, demonstrating that both Gr and Tr are multi-layer graphene films. Raman spectra also reveal the signal of typical multi-layer graphene, i.e., 2D band (~2700 cm<sup>-1</sup>) is lower than G band (~1580 cm<sup>-1</sup>),<sup>27</sup> as shown in Fig. 1f and i.

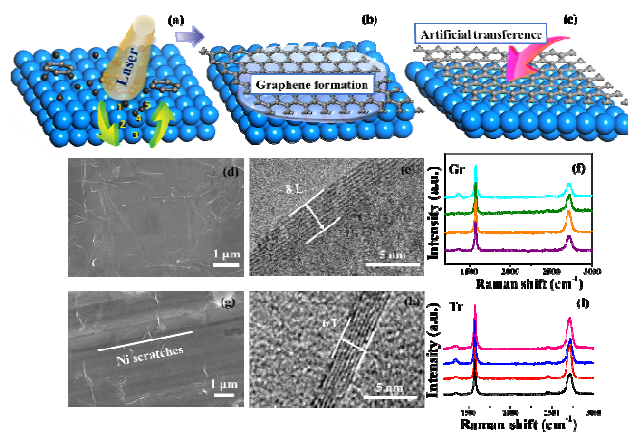


**Fig. 1** (a) and (b) Schematic of graphene formation by laser process; (c) Schematic of graphene transferred onto the Ni substrate; (d) and (g) field emission SEM images of graphene on nickel. (e) and (h) high resolution TEM images of different edges. (f) and (i) 514 nm Raman spectra of graphene in random locations. (d)-(f) results for *in-situ* grown graphene (labelled “Gr”). (g)-(i) results for transferred graphene (labelled “Tr”).

### Polarization analysis

The corrosion behaviours of the bare nickel (labelled “Bare Ni”), the samples with transferred graphene via CVD onto a nickel surface (labelled “Tr”), and the samples with *in-situ* grown graphene by laser process on a nickel surface (labelled “Gr”) were analysed as follows. An electrochemical reaction under activation control obeys the Butler-Volmer equation, which relates the exponential dependence of current to the deviation of potential from the open circuit potential value.<sup>14,15,23-25</sup> Using the potentiodynamic measurements to quantify the corrosion behaviour, the logarithm of the current density ( $\log i$ ) vs. the electrode potential ( $E$ ) could be plotted. Each experiment was repeated 3 times to evaluate reproducibility. Fig. 2f-h presents one group of polarization curves. Based on the “theory” part, we can obtain the important corrosion relative parameter, such as  $E_{corr}$  and CR. The original data of all the parameter are listed in Table S1 (see Supplementary Information). Here, we mainly focused on the corrosion rate and corrosion potential of different samples, as shown in Fig. 2i and j.

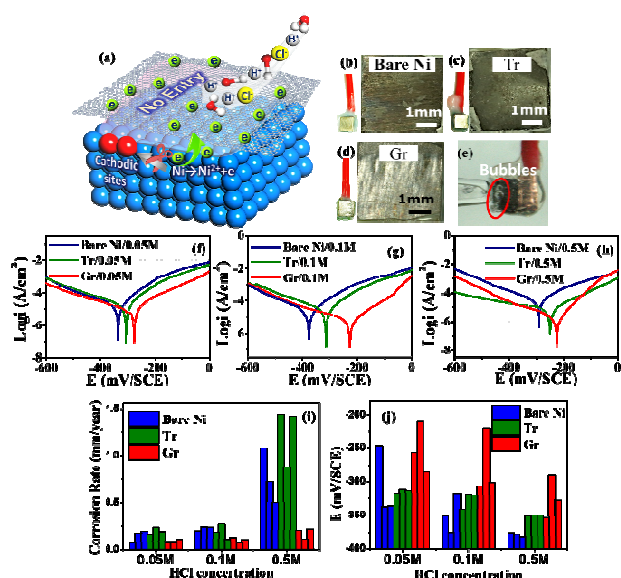


**Fig. 2** (a) Schematic of anti-corrosion mechanism of graphene. (b)-(d) Topographies of Bare Ni, Tr and Gr after 0.5 M HCl corrosion measurement. (e) Bubbles during corrosion measurement; (f)-(h) Polarization curves in 0.05 M (f), 0.1 M (g) and 0.5 M (h) HCl (aq). (i) Corrosion rate and (j) corrosion potential of bare Ni, Tr and Gr in HCl (aq).

Fig. 2i shows the corrosion rate of bare Ni, Tr and Gr in different HCl solutions. In the lowest concentration (0.05 M), all the samples of bare Ni, Tr and Gr maintain the low corrosion rate. However, the corrosion rate of Gr is still less than those of bare Ni, and the average corrosion rate of bare Ni is 1.8 times of Gr, while the CR values of Tr are slightly higher than those of bare Ni. The anti-corrosion situation in 0.1 M HCl (aq) is familiar with the former group. Compared to bare Ni and Tr, the *in-situ* grown graphene exhibits better anti-corrosion capability as evidenced by the lowest values of corrosion rate. In 0.5 M HCl solution, it can be seen that bare Ni and Tr was corroded very fast, evidenced by the high corrosion rate. However, the corrosion rates of Gr still stay in the low level, only one quarter of that of bare Ni. As the concentrations increased, all the CR values of different samples increased.

Fig. 2j provides the comparison of corrosion potentials. The corrosion potential is regarded as the threshold value of reactions between the metal and the environment. A higher  $E_{\text{corr}}$  means better corrosion resistance. In all three different concentrations, Gr has the highest  $E_{\text{corr}}$  (126 mV higher than bare Ni), which means the best resistance to the corrosive environment. Unlike the situation of corrosion rate, the potential values of Tr are slightly higher than those of bare Ni, implying that Tr is better than bare Ni to resist the corrosive solutions. The inconsistent results of Tr show that the transferred graphene had the ability to resist the acid solution, so it has a higher  $E_{\text{corr}}$ . However, the ability becomes invalid with prolong of time, due to exfoliation of transferred graphene from the surface, so CR is also high. All the above analyses demonstrate that the graphene grown by laser irradiation performs superiorly at resisting the HCl corrosive environment.

In brief, the polarization results show that (i) the *in-situ* grown graphene performed superiorly at resisting the HCl corrosive environment; (ii) the protection for Ni substrate by *in-situ* grown graphene is much more effective in higher concentration; (iii) the transferred graphene cannot improve the corrosion resistance of bare Ni, even performs worse than bare Ni in 0.5 M HCl.

Next, we will discuss the protection mechanism of the *in-situ* grown graphene and transferred graphene. The anti-corrosion mechanism provided by graphene can be explained as follows:<sup>28</sup> (i) graphene tends to make the path of permeating water more tortuous; (ii) because of the impermeability of pristine graphene, it can act as an excellent barrier to the harmful ions, as shown in Fig. 1a, including  $H^+$ ,  $OH^-$  and  $Cl^-$ . However, for Tr, there remain a sizable gap between nickel and graphene, and no interaction could be established.<sup>29, 30</sup> In this case, the solution could penetrate the interface between the transferred graphene and nickel, and then  $H^+$  reacts with Ni to produce hydrogen bubbles in the interface, as shown in Fig. 2e. As the hydrogen bubbles increase, the gap becomes bigger so that the graphene tends to move away from the nickel surface. This process has also been used to exfoliate the CVD-grown graphene from Cu foils.<sup>31</sup> In brief, the transferred graphene cannot stay on the surface steadily. The higher corrosion rates of Tr than those of bare Ni can be explained by the galvanic cells formed between transferred graphene and Ni substrate. These cells accelerated the corrosion of Ni substrate. For *in-situ* grown graphene by laser, the excellent anti-corrosive quality can be attributed to the strong interaction between graphene and nickel. During *in-situ* growth by laser, the carbon atoms were dissolved into the molten Ni and then precipitated out onto the surface to form the graphene film. Under this growth mechanism, the graphene had a good adhesion with the substrate.<sup>15,32</sup> For more supporting information, we characterized the surface damage (Fig. 2b-d and Fig. 3) and structure change (Fig. 4) after polarization measurements, and conducted immersion test to evaluate the corrosion evolution with time.

#### Surface damage after polarization measurement

Fig. 2b-d shows the photos of bare Ni, Tr and Gr after 0.5 M HCl (aq) corrosion. More details are given in Fig. 3. The extent of the corrosive damage of the bare Ni is shown in Fig. 3b-e. The original nickel has some polishing scratches on the surface. After 0.05 M HCl etching, the surface has changed, but the polishing scratches can be still distinguished. Upon further increase in concentration of  $Cl^-$  and  $H^+$ , the scratches are gone completely, due to the corrosion of nickel and evolution of hydrogen happened on the surface as shown in Fig. 3a. The original transferred graphene on nickel surface can be observed in Fig. 3g and the inset. Then we cannot find any graphene after polarization measurements, as shown in Fig. 3h and j. For *in-situ* grown graphene on nickel surface, the graphene wrinkles can be observed clearly in Fig. 3l and the inset. The distinct topography of graphene has been maintained invariably after

corrosion reactions (see Fig. 3m-o), with the exception of some cracks being sparsely generated.

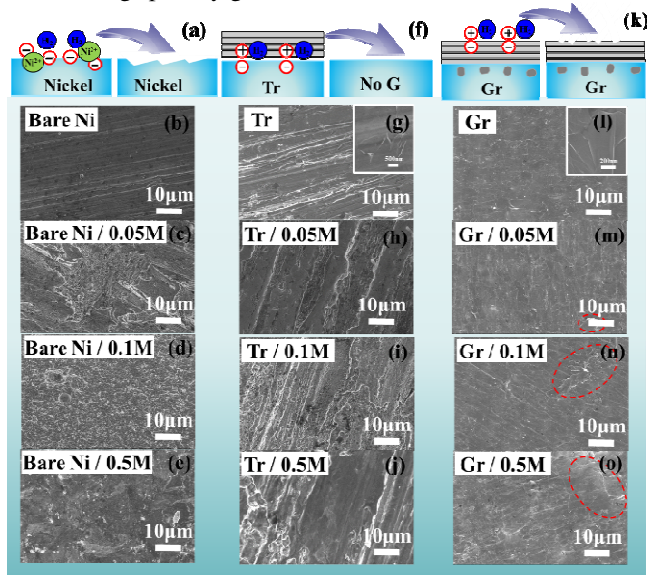


**Fig. 3** (a) Corrosion of bare Ni; (b)-(e) SEM images of bare Ni before and after corrosion tests. (f) Corrosion of Tr; (g)-(j) SEM images of Tr. (k) Corrosion of Gr; (l)-(o) SEM images of Gr. The insets of (g) and (l) give the details of graphene wrinkles by magnified view. The red dotted circles marks the cracks on the graphene in (m)-(o).

#### Structure change after polarization measurement

Raman mapping of  $I_D/I_G$  were used to further understand the graphene films after electrochemical corrosion. Fig. 4a-h display the mapping results in an area of  $254 \times 25 \mu\text{m}^2$  of Tr and Gr, respectively. Fig. 4i and j show the Raman spectra of different samples. The  $I_{2D}/I_G$ s can be obtained from these spectra. Ferrari *et al.*<sup>27</sup> pointed out that G band ( $\sim 1580 \text{ cm}^{-1}$ ) reflects the doubly degenerate zone centre  $E_{2g}$  mode while D band ( $\sim 1350 \text{ cm}^{-1}$ ) indicates the absence of a significant number of defects, and the 2D band ( $\sim 2700 \text{ cm}^{-1}$ ) provides information about the number of layers. The increase in layers leads to a significant decrease of the relative intensity of 2D ( $I_{2D}$ ) with a blue shift. Therefore,  $I_D/I_G$  can reflect the extent of the damage and  $I_{2D}/I_G$  can be used to identify the layer number of graphene cursorily. It can be seen by the colour bar that the blue areas have less defects and the orange areas were damaged more seriously. Both original Tr and Gr are multi-layer graphene films with less defects as shown in Fig. 4a, e, i, and j. In HCl solutions, the  $I_D/I_G$ s of Tr increase obviously in Fig. 4a-d. Meanwhile, the  $I_D/I_G$ s of Gr remain the same level with the original one after electrochemical reactions (see Fig. 4e-h). The Raman spectra were extracted from the mapping. It can be seen in Fig. 4i that the spectrum of Tr in 0.05 M HCl has D, G and 2D peak, but it is far from the typical graphene feature. The 2D peaks of Tr in 0.1 and 0.5 M HCl have almost disappeared, meaning there is no graphene here. For Gr, the graphene feature has been reserved very well after tests as shown in Fig. 4j. Raman analyses conform to the observation of SEM. The

statement, the transferred graphene has been removed away, while the *in-situ* grown graphene has been reserved, has been proved once again.

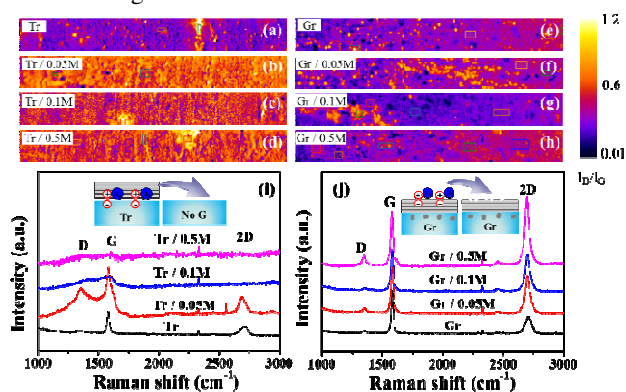


**Fig. 4** Raman analyses. (a)-(h) 532 nm Raman mapping of  $I_D/I_G$  in the area of  $254 \times 25 \mu\text{m}^2$ . (i) and (j) Raman spectra of Tr and Gr before and after electrochemical corrosion measurement.

#### Immersion measurements

To further understand the anti-corrosion performance of graphene with time, here we immersed the samples into a much harsh etching solution, 0.5 M  $\text{FeCl}_3/\text{HCl}$  (aq). Only the top surface was exposed to the solution, and other surface was sealed by sealant. Fig. 5 shows the topography changing with time. After 5 min immersion, bare Ni and Tr began to be corroded (Fig. 5b and g), while Gr maintained the original surface topography. After immersion for 15 min, bare Ni was corroded severely (Fig. 5c). Compared to bare Ni, Tr was less corroded (Fig. 5h), but some floating graphene debris were observed above the Tr (Fig. 5q), indicating that the transferred graphene had moved away from the Tr surface. For Gr, the surface still maintained the original features. After 30 min immersion, the surface of bare Ni was totally damaged (Fig. 5c), and a large-area corrosion happened on the surface of Tr (Fig. 5i). There were several tiny cracks observed in Gr surface, as shown in Fig. 5n. Further extending the immersion time to 120 min, the corrosion of bare Ni and Tr happened not only on the surface but into the internal along the grain boundaries, as seen in Fig. 5e and j. For Gr, the cracks were propagated to some bigger cracks. These cracks did not destroy the whole graphene film until 24 h immersion, as shown in Fig. 5p. Based on the immersion results, in this harsh solution, bare Ni and Tr could not resist corrosion for more than 15 min, while the *in-situ* grown graphene could protect the underlying substrate for 24 h.

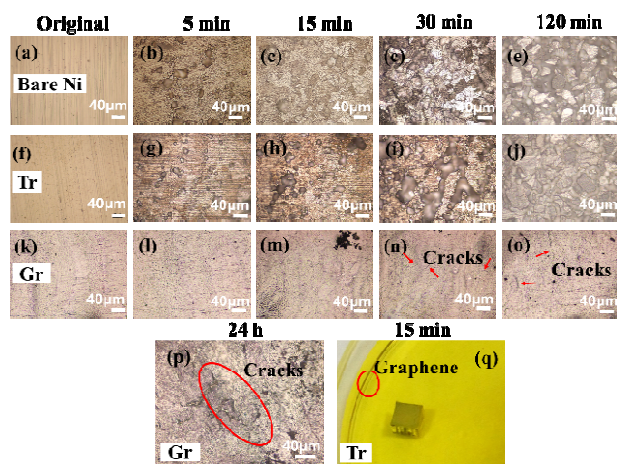


**Fig. 5** Optical images after immersion tests. (a)–(e) The topographies of Bare Ni at different immersion time, original, 5 min, 15 min, 30 min, and 120 min. (f)–(j) The topographies of transferred graphene. (k)–(o) The topographies of *in-situ* grown graphene. The arrows mark the cracks. (p) The topographies of *in-situ* grown graphene after 24 h immersion. The circle shows the crack area. (q) The photo of Tr in etching solution. The circle shows the graphene moved from the surface of Tr.

Compared to potentiodynamic polarization, EIS enables to obtain information on the corroding surface without introducing a substantial perturbation to the corrosion process. Here, EIS was used to complement the findings from the other corrosion testing methods and obtain further qualitative information on the anticorrosion performance provided by the graphene layers. Typical EIS spectra obtained in the 0.5 M HCl electrolyte are presented in Fig. 6. Three regions are clearly evident in the spectra: i) a high frequency region where the effects associated to the solution resistance and parasitic inductance of the cables dominates, ii) a medium-frequency region, dominated by the capacitive behaviour due to charge separation at the metal/(graphene)/electrolyte, and iii) a low frequency region where charge-transfer and diffusion-related phenomena prevail. For the purpose of the present work, regions ii) and iii) are of main interest. At medium frequencies, a shift in the curves towards the right is associated to a decrease in the overall capacitance. In corrosion terms, high values of capacitance are regarded as problematic, since they indicate that a double-layer capacitance is present on the corroding surface, *i.e.* the electrolyte is in contact with the metal and corrosion is occurring. On the other hand, considering that the capacitance is inversely proportional to the distance of charge separation, a decrease in value of capacitance is generally associated to the presence of a protective layer between the metal and the electrolyte. From the EIS spectra acquired, it is evident that the electrode that supports the *in-situ* grown graphene display the lower value of overall capacitance, indicating that the graphene layer is effective in providing separation between the metal and the corrosive environment. Close scrutiny of the low-frequency region of the impedance spectra indicates that inductive contributions, more marked for the *in-situ* grown graphene are

revealed by EIS analysis. The exact origin of the inductive behaviour has not been investigated here but, qualitatively, the significantly higher value of impedance modulus for the specimen supporting *in-situ* grown graphene confirms that this has considerably higher corrosion resistance compared to the other two specimens. Overall, the impedance results, together with the potentiodynamic polarization results, suggest that the *in-situ* grown graphene behaves as a barrier layer that prevents direct contact between metal and electrolyte, thereby limiting the anodic reaction rate.

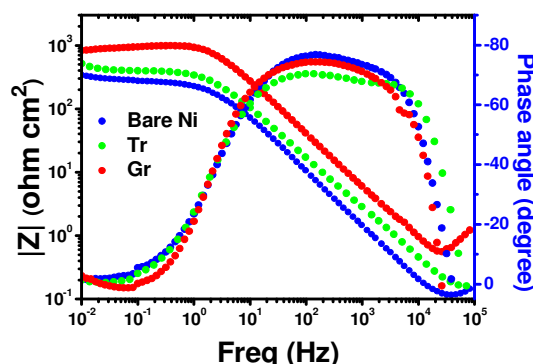


**Fig. 6.** EIS results (Bode plots) of bare Ni, Tr and Gr after 1 h immersion in 0.5 M HCl.

## Conclusions

Graphene as a protective coating on nickel has been investigated by polarization analysis and immersion measurement. We have compared three groups of samples, bare Ni, transferred graphene, and *in-situ* grown graphene. Considering the passivation of nickel in alkaline solution, HCl were used as the corrosive solutions. Polarization curves and the electrochemical corrosion reaction parameters indicated that the *in-situ* grown graphene had a superior anti-corrosion performance than bare Ni and Tr. The corrosion rate was 4.5 times lower than that for bare Ni, and the corrosion potential was increased of 126 mV. From the post-corrosion micrographs, it is evident that Gr maintained the original topography while the other specimens were damaged. Raman mapping results showed that there was no graphene on the surface after the corrosion tests of Tr but, for Gr, the graphene remained after the tests. The immersion results and EIS results showed that, in this harsh solution, bare Ni and Tr could not resist the corrosion very well, while the *in-situ* grown graphene could protect the underlying substrate effectively, due to its strong interaction with substrate, high conductivity and excellent impermeability.

## Acknowledgements

The authors greatly thank the funding support by China National Key Basic Research and Development Program (2011CB013000).

## Notes and references

<sup>a</sup> School of Materials Science and Engineering, Tsinghua University, Beijing, 100084, China

Corresponding Author: Minlin Zhong, zhml@tsinghua.edu.cn

<sup>b</sup> Corrosion Protection Centre, School of Materials, The University of Manchester, Manchester, M13 9PL, UK

Electronic Supplementary Information (ESI) available: [Electrochemical corrosion reaction kinetic parameters]. See DOI: 10.1039/b000000x/

- 1 J. Zhu, S. Wei, I. Y. Lee, S. Park, J. Willis, N. Haldolaarachchige, D. P. Young, Z. Luo, Z. Guo, *RSC ADV.*, 2012, **2**, 1136.
- 2 R. Kasemann, H. Schmidt, *NEW J. CHEM.*, 1994, **18**, 1117.
- 3 R. B. Mester, A. Steffens, US Pat., 13/812, 910, 2011-7-20.
- 4 K. S. Novoselov, V. I. Fal'ko, L. Colombo, P. R. Gellert, M. G. Schwab, K. Kim, *NATURE*, 2012, **490**, 192.
- 5 K. S. Kim, Y. Zhao, H. Jang, S. Y. Lee, J. M. Kim, K. S. Kim, J. H. Ahn, P. Kim, J. Y. Choi, B. H. Hong, *NATURE*, 2009, **457**, 706.
- 6 C. R. Dean, A. F. Young, I. Meric, C. Lee, L. Wang, S. Sorgenfrei, K. Watanabe, T. Taniguchi, P. Kim, K. L. Shepard, J. Hone, *NAT. NANOTECHNOL.*, 2010, **5**, 722.
- 7 A. K. Geim, K. S. Novoselov. *NAT. MATER.*, 2007, **6**, 183.
- 8 L. G. De Arco, Y. Zhang, C. W. Schlenker, K. Ryu, M. E. Thompson, C. W. Zhou, *ACS NANO*, 2010, **4**, 2865.
- 9 X. An, C. Y. Jimmy, *RSC ADV.*, 2011, **1**, 1426.
- 10 N. Zhang, Y. Zhang, Y. J. Xu, *NANOSCALE*, 2012, **4**, 5792.
- 11 J. S. Bunch, S. S. Verbridge, J. S. Alden, A. M. Van der Zande, J. M. Parpia, H. G. Craighead, H. G. Craighead, P. L. McEuen, *NANO LETT.*, 2008, **8**, 2458.
- 12 S. Chen, L. Brown, M. Levendorf, W. Cai, S. Y. Ju, J. Edgeworth, C. M. Li, C. Magnuson, A. Velamakanni, R. R. Piner, *ACS NANO*, 2011, **5**, 1321.
- 13 P. K. Nayak, C. J. Hsu, S. C. Wang, J. C. Sung, J. L. Huang, *THIN SOLID FILMS*, 2013, **529**, 312.
- 14 C. H. Chang, T. C. Huang, C. W. Peng, T. C. Yeh, H. I. Lu, W. I. Hung, C. J. Weng, T. I. Yang, J. M. Yeh, *CARBON*, 2012, **50**, 5044.
- 15 D. Prasai, J. C. Tuberquia, R. R. Harl, G. K. Jennings, K. I. Bolotin, *ACS NANO*, 2012, **6**, 1102.
- 16 F. Zhou, Z. T. Li, G. J. Shenoy, L. Li, H. T. Liu, *ACS NANO*, 2013, **7**, 6939.
- 17 S. Mayavan, T. Siva, S. Sathiyarayanan, *RSC ADV.*, 2013, **3**, 24868.
- 18 A. S. Kousalya, A. Kumar, R. Paul, D. Zemlyanov, T. S. Fisher, *CORROS. SCI.*, 2013, **69**, 5.
- 19 M. Topsakal, H. Şahin, S. Ciraci, *PHYS. REV. B.*, 2012, **85**, 155445.
- 20 X. Ye, J. Long, Z. Lin, H. Zhang, H. Zhu, M. Zhong, *CARBON*, 2014, **68**, 7840.
- 21 I. Heller, J. Kong, K. A. Williams, C. Dekker, S. G. Lemay, *J. AM. CHEM. SOC.*, 2006, **128**, 7353.
- 22 Y. Shao, J. Wang, H. Wu, J. Liu, I. A. Aksay, Y. Lin, *ELECTROANAL.*, 2010, **22**, 1027.
- 23 M. Coros, A. R. Biris, F. Pogacean, L. B. Tudoran, C. Neamtu, F. Watanabe, A. S. Biris, S. Pruneanu, *ELECTROCHIM. ACTA*, 2013, **91**, 137.
- 24 R. K. S. Raman, P. C. Banerjee, D. E. Lobo, H. Gullapalli, M. Sumandasa, A. Kumar, L. Choudhary, R. Tkacz, P. M. Ajayan, M. Majumder, *CARBON*, 2012, **50**, 4040.
- 25 J. H. Huh, S. H. Kim, J. H. Chu, S. Y. Kim, J. H. Kim, S. Y. Kwon, *NANOSCALE*, 2014, **6**, 4379.
- 26 S. J. Chae, F. Gunes, K. K. Kim, E. S. Kim, G. H. Han, S. M. Kim, H. J. Shin, S. Yoon, J. Choi, M. H. Park, C. W. Yang, D. Pribat, Y. H. Lee, *ADV. MATER.*, 2009, **21**, 2328.
- 27 A. C. Ferrari, J. C. Meyer, V. Scardaci, C. Casiraghi, M. Lazzeri, F. Mauri, S. Piscanec, D. Jiang, K. S. Novoselov, S. Roth, A. K. Geim, *PHYS. REV. LETT.*, 2006, **97**, 18740118.
- 28 S. Böhm, *NAT. NANOTECHNOL.* 2014, **9**, 741.
- 29 R. W. Havener, H. Zhuang, L. Brown, R. G. Hennig, J. Park, *NANO LETT.*, 2012, **12**, 3162.
- 30 X. H. Ye, T. Huang, Z. Lin, M. L. Zhong, L. Li, Y. Z. Yan, H. W. Zhu, *CARBON*, 2013, **61**, 329.
- 31 L. Gao, W. Ren, H. Xu, L. Jin, Z. Wang, T. Ma, L. Ma, Z. Zhang, Q. Fu, L. Peng, X. Bao, H. M. Cheng, *NAT. COMMUN.*, 2012, **3**, 699.
- 32 R. K. S. Raman, A. Tiwari, *JOM*, 2014, **66**, 637.
- 33 W.S. Tait, *Racine, WI: Pair O Docs Publications*, 1994, ch. 8, pp. 100.